Development and Evaluation of New Methods for Estimating Albedo-area for Stable Geos

**Tamara E. Payne, Stephen A. Gregory, Anthony Dentamaro, Markus Ernst,
Jeffrey Hollon, Adam Kruchten, Anil B. Chaudhary**
Applied Optimization
714 East Monument Ave, Suite 204
Dayton, OH 45402
Phan D. Dao
AFRL/RVBY
3550 Aberdeen Ave. SE
Kirtland AFB, NM 87117-5776

ABSTRACT

Although direct measurements of the projected areas of various Geosynchronous Earth Orbit (GEO) satellite facets are impossible without high-resolution imaging, estimates of the albedo-Area (aA) product lead to the possibility of inferring the area. Such size estimates are an integral part of its identity. We are engaged in parallel development of two methods for calculating aA for the body/communication antennae structures and one method for the solar panels. We have previously reported on the Two Facet Model (2FM) method for body aA, and here we discuss a method based on differences between new observations and a baseline catalog that has been constructed from the GEO Observations with Longitudinal Diversity Simultaneously (GOLDS) data. We report on evaluations of the 2FM and differential method (DM) algorithm results. We also discuss a new method of estimating solar panel aA by fitting new data that include specular glints. All of these measurement methods are compared to models and simulations that serve as a proxy for ground truth. Because of the partially directional nature of the composite Bi-directional Reflectivity Distribution Function (BRDF) of all bus-mounted appendages, variance of body aA results is expected to be significant. Short-term and long-term variance of the derived aAs will also be discussed.

1. INTRODUCTION

We have been conducting both observational and analysis programs for geostationary satellites. The primary databases that we have created and used for algorithmic development are the Geo Color Photometry Catalog (GCPC, Gregory and Payne) and the Geo Observations with Longitudinal Diversity Simultaneously (GOLDS, Gregory, et al). The observations were carried out with a variety of commercial, off-the-shelf (COTS), Raven-like sensors that are primarily located in continental US (CONUS) and Maui. The photometric observations were obtained through the Johnson (or its derivatives) filter system, with most of the data being in the B and R filters, thus providing both brightness and color information. Several analyses of the data have been conducted and show, among other important findings, that there are important diurnal, seasonal, and geographic dependences of both brightness and color. The research presented here is aimed at deriving effective estimates of the sizes of these objects by calculating the albedo-Area (aA) products of the bus/payload/com antennae and solar panels based on "new data", using the GCPC and GOLDS catalogs to develop our algorithms. In general, these new methods can be used with any new ground- or space-based sensors and can be generalized to different filter/detector combinations.

2. SATELLITE-BASED COORDINATES

One of our goals has been to remove as much of the sensor location and seasonal variations as possible by carrying out our calculations in a coordinate system that is based on the Resident Space Object (RSO) itself. The manner in which these ground-based geographic and seasonal effects contribute to observed brightness is determined from the calculation of several body frame angles.

In defining the RSO reference frame, it is assumed the Geo object is in a nadir-aligned stabilization (i.e., the normal of the nadir-facing facet is anti-parallel to the vector that points from Earth center to the satellite). Fig. 1 shows the geometry of the RSO coordinate frame. The surface represents the nadir-pointing facet of the object, and we identify the surface normal **n** with the body axis z_B. For a satellite in orbit, the direction of its velocity vector, $|\mathbf{v}|$, lies in the orbital plane, as does **n**, and so the cross product **n** x $|\mathbf{v}|$ is normal to **n** and points to orbital South. We identify this

vector as y_B. If the object is in a perfectly circular orbit ($e \equiv 0$), the velocity vector $\mathbf{v}$ would complete the triad, and the body frame would be complete; however, for $e \neq 0$, the third reference frame axis, x_B, is defined by $y_B \times z_B \equiv (\mathbf{n} \times |\mathbf{v}|) \times \mathbf{n}$.
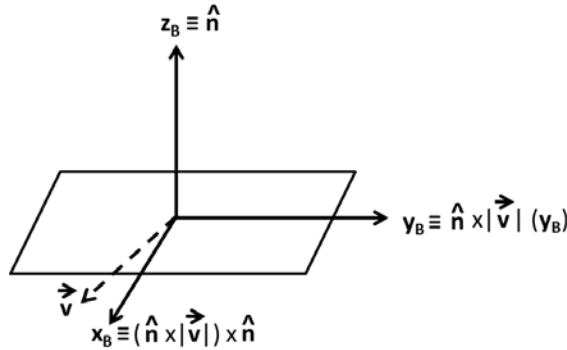

Fig. 1 Definition of RSO coordinate frame

Fig. 2 shows the four body angles that will be used in the work described herein; these are the Sun zenith and azimuthal angles (θ_s, Φ_s, respectively) and observer zenith and azimuthal angles (θ_o, Φ_o, respectively). Zenith angles are the separations between the surface normal and the vectors that point to the Sun or observer. Azimuthal angles are measured between one of the axes (x_B, in the figure) and the projection of the Sun, or observer, vector onto the facet surface. The sign of these angles (i.e., the direction of rotation from the x_B axis) must be taken into account. For our purposes, one only needs to calculate $|\Delta\Phi_o| = |\Phi_s - \Phi_o|$, the absolute angular difference between the projections of the Sun and observer vectors.
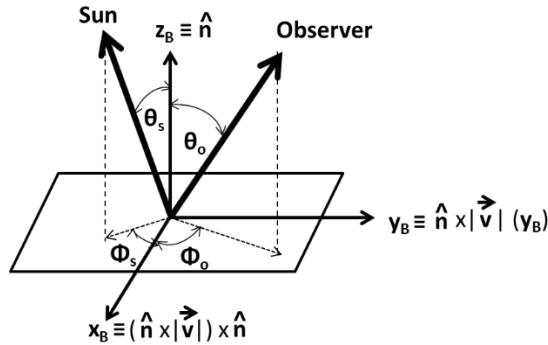

Fig. 2 Definition of body angles in RSO coordinate frame

3. THE TWO FACET MODEL (2FM) METHOD FOR BODY aA

The measured brightness of an RSO can be decomposed into the contribution due to the RSO solar panel and the contribution due to the RSO bus. Following the assumptions that the solar panel tracks the sun (possibly with an offset) and that the bus tracks nadir, the dynamics of a RSO can be approximated with a two-facet model. One facet in the model represents the RSO solar panel and tracks the sun. This facet is assumed to be approximately planar and is assumed to have both specular and Lambertian reflective properties. As the solar panel is assumed to be planar, it is decomposed into a singular albedo-Area product. The second facet of the model represents the RSO bus. The bus is assumed to be nadir pointing and is a complex three-dimensional shape. The bus is assumed to exhibit primarily Lambertian reflectance but is further assumed to have reflective properties that are pose-dependent relative to the sun and observer. Due to this pose-dependence, the RSO bus is thus decomposed into a number of different albedo-Area products to accommodate differential albedo-Areas under different observation conditions.

At present the method for solving for the various albedo-Area products of the bus is reviewed. A method for integrating the various albeda-Area products into a single average albedo-Area product for the RSO bus is additionally discussed. The method for solving for the albedo-Area products of the RSO bus leverages the assumed Lambertian reflectance

of the bus to represent the albedo-Area products in terms of a system of linear equations which can be efficiently solved. In contrast to the bus, the specular nature of the solar panel's reflectance requires the reflectance be modeled in terms of a function that has high reflective properties near the point of ideal specular reflection and low reflective properties further away. The specular nature of the Solar Panel's reflectance requires the usage of a non-linear shape parameter. Due to this introduced non-linearity, the current method cannot be applied to the solar panel. An alternative method for computing the albedo-Area of the solar panel is later discussed in Section 6. As such, the current discussion concerns the decomposition of the body contribution to a signature into a number of pose-dependent albedo-Areas.

The RSO bus is modeled with a Lambertian basis function. That is, the projected albedo-Areo of the RSO bus is proportional to $\cos(\theta_s)\cos(\theta_o)$ where θ_s is the angle between the RSO-nadir vectors and the sun, and θ_o is the angle between the RSO-nadir vector and the observer. As the observed brightness of the bus is assumed to be pose dependent, the bus is modeled with multiple basis functions multiplied by participation factors $b_i(\gamma)$ which are functions of the orbital angle γ. The particular choices of participation factors b_i are somewhat arbitrary; however, here they are assumed to be piecewise continuous linear functions. For the bus, then, the total projected albedo-Area $\widetilde{aA_{BUS}}$ is a sum of the projected albedo-Areas across all orbital angle ranges:

$$\widetilde{aA_{BUS}} = \sum_{i=1}^{k} aA_i \cos(\theta_s)\cos(\theta_o)b_i(\gamma) \tag{1}$$

aA_i is the in-orbital angle albedo-Area of the RSO bus, and k is the total number of orbital angle bins. The above equation is linear in terms of unknown coefficients aA_i. Thus the parameters can be solved for by constructing a linear system of equations:

$$X\beta = Y \tag{2}$$

X is a design matrix of basis functions per orbit angle bin:

$$X = \begin{bmatrix} \cos(\theta_{i1})\cos(\theta_{o1})\,b_1(\gamma_1) & \cos(\theta_{i1})\cos(\theta_{o1})\,b_2(\gamma_1) & \cdots & \cos(\theta_{i1})\cos(\theta_{o1})\,b_k(\gamma_1) \\ \cos(\theta_{i2})\cos(\theta_{o2})\,b_1(\gamma_2) & \cos(\theta_{i2})\cos(\theta_{o2})\,b_2(\gamma_2) & \cdots & \cos(\theta_{i2})\cos(\theta_{o2})\,b_k(\gamma_2) \\ \vdots & \vdots & \ddots & \cdots \\ \cos(\theta_{in})\cos(\theta_{on})\,b_1(\gamma_n) & \cos(\theta_{in})\cos(\theta_{on})\,b_n(\gamma_n) & \cdots & \cos(\theta_{in})\cos(\theta_{on})\,b_k(\gamma_n) \end{bmatrix} \tag{3}$$

β is a column vector of the unknown aA_i, and Y is a column vector of observed projected albedo-Areas. The ordinary least squares solution can then be computed as $\beta = pinv(X)Y$ where $pinv$ represents the Moore-Penrose pseudoinverse $pinv(X) = (X^T X)^{-1} X^T$, giving the desired result.

Now that we have shown how to compute a vector of pose dependent albedo-Areas, we will discuss how to convert this vector into a singular albedo-Area value to represent the satellite as a whole. We wish to obtain a single aA value because it is easier for an analyst to work with one value rather than a vector of values. It is also easier to perform change detection using one aA value rather than the entire vector.

The method we use is as follows:

We only use the lambertian observations with γ(orbit angle) values in [-75, 75] to calculate the body diffuse aA. There are 11 orbit angle bins, each spanning 15 ($BinSize$) degrees measured in γ. From the previous steps, we obtain β which holds 11 aA values.

$$BinSize = 15$$

$$n = \#\ of\ observation$$

$$<variable>_i = subscript\ i\ represent\ the\ value\ of\ <variable>\ for\ observation\ i$$

$$w_{iL} = \left\lfloor \left(\frac{\gamma_i}{BinSize}\right)\right\rfloor - \left(\frac{\gamma_i}{BinSize}\right)$$

$$w_{iR} = \left\lceil \left(\frac{\gamma_i}{BinSize}\right)\right\rceil - \left(\frac{\gamma_i}{BinSize}\right)$$

$$aA_{iL} = \beta_{\left\lfloor\left(\frac{\gamma_i}{BinSize}\right)\right\rfloor}$$

$$aA_{iR} = \beta_{\left\lceil\left(\frac{\gamma_i}{BinSize}\right)\right\rceil}$$

$$Body\ diffuse\ aA = \frac{\sum_{i=1}^{n} w_{iL} * aA_{iL} + w_{iR} * aA_{iR}}{\sum_{i=1}^{n} \cos(\theta_{s_i}) * \cos(\theta_{o_i})} \qquad (4)$$

4. THE DIFFERENTIAL METHOD (DM) FOR BODY aA

Many of our methods treat a signature as the primary analysis source. In our usage, "signature" refers to a plot of brightness or color index vs. the longitudinal component of the total sensor/RSO/sun Phase Angle (LPA or just PA). $PA = 0^o$ is defined when the object lies directly opposite the sun in its diurnal motion. Hence negative PA values occur earlier in the night, and positive PA values occur later. An experienced analyst can qualitatively extract a number of important features from a signature, and we are continuing development to automate these kinds of analyses. For example, a signature can provide information about the offset of the solar panels from their nominal direction of pointing at the sun. It can also often provide the number and placement of large communication (com) antennae. Since different manufacturer/bus types tend to have self-consistent offsets and large structures, signature types are correlated with manufacturer/bus types.

As examples, we present Fig. 3 and Fig. 4, which illustrate simple and complex signature types, respectively. In both plots, we use the range corrected (36,000 km) Johnson R band magnitudes (i.e., R_{abs}, to indicate brightness). We note that all of the DM analysis presented here will use R_{abs}. The reason for concentrating on the R band observations is that we are trying to analyze the portions of the RSO that do not include the solar panels, which are brightest in the blue. Especially near glint season, signatures are dominated by the central PA regions where the solar panels are brightest. Note that the DTV-10 (bus type Boeing Space Systems 702) signature in Fig. 3 shows only one brightness peak that is located near $PA = 0^o$ and has monotonically decreasing brightness on either side. In contrast, Fig. 4 presents the signature of SES-1 (bus type STAR 2), and one can see shoulders, which are located between 30° and 40° on either side of the central peak, which, in this case, is offset by about 8° from the sun (i.e., the solar panel normal is offset by about 4° from the direction to the sun). At some times during the year, as seasonal illumination conditions vary, these shoulders turn into broad peaks. Our interpretation of these shoulders and side peaks is that they arise from diffuse reflections from large com antennae, with the peak at negative PA arising from an antenna located on the eastern or leading side of the satellite.
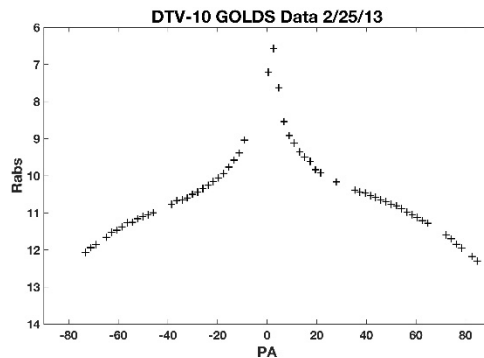

Fig. 3 Example signature – DTV-10, showing a single peak
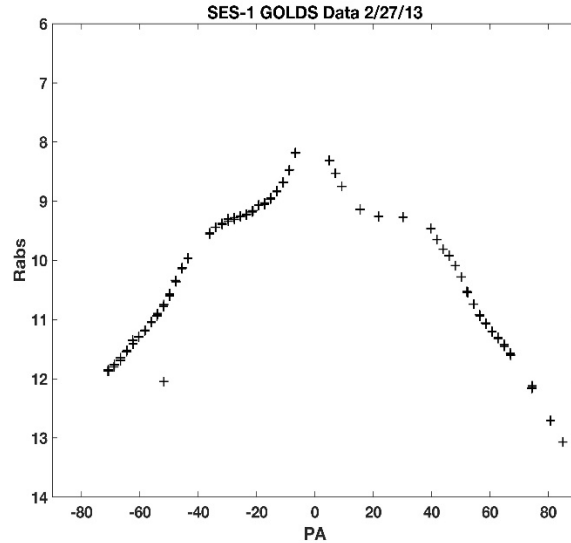
SES-1 GOLDS Data 2/27/13

Fig. 4 Example signature – SES-1, showing a peak with two shoulders

We have pointed out the degree of complexity of signatures because this is an important consideration in applying the DM method. We use the brightness information in the range abs(PA) > 40º in the body aA calculation. In the RSO-based coordinate system discussed in Section 2, this is also approximately the same range in $\Delta\Phi$ at these angles that lie far from 0º. To emphasize these points, note that the brightness in the PA > 40º range is higher for the complex-signature satellites than that of the simple-signature satellites, and we allow for this natural difference in our DM method.

The Differential Method is based on determination of the mean difference in magnitude between the new observations of a satellite and a baseline catalog for that satellite's signature type. These catalogs were built up from observations taken during the GOLDS project, in which multi-site observations were made in 2013. They feature many exposures per night in B and R. We have constructed four baseline catalogs—that of the Single Peak, the Double Peak (Left), the Double Peak (Right), and the Triple Peak objects. Double Peak (Left) signatures have a single com antenna whose corresponding brightness peak is usually somewhat lower than the central peak, which is generally caused by specular or near specular reflections from the solar panels and are located typically in the range -10º < PA < +10º. The lower, broad side peaks tend to be located in the range 30º < abs(PA) < 40º. The Double Peak (Right) signatures are essentially mirror reflection of the Double Peak (Left) signatures. The Triple Peak signatures show evidence for peaks at both negative and positive PAs.

Fig. 5 presents the magnitude and body-referenced angle information found in the baseline catalogs. For illustrative purposes, we have added all of the catalogs together. There are two main groupings in the $\Delta\Phi$ coordinate, and the noticeable tracks that lie at a nearly constant value of $\Delta\Phi$ but move from front left to back right in θ_s are the trajectories that the data takes when observations are taken many times throughout a single night. The two groupings (roughly half positive and half negative) in $\Delta\Phi$ represent the positive and negative portions of the Phase Angle distribution, i.e., those observations made prior to the moment of 0º PA (the positive $\Delta\Phi$ values) and those made after 0º PA.
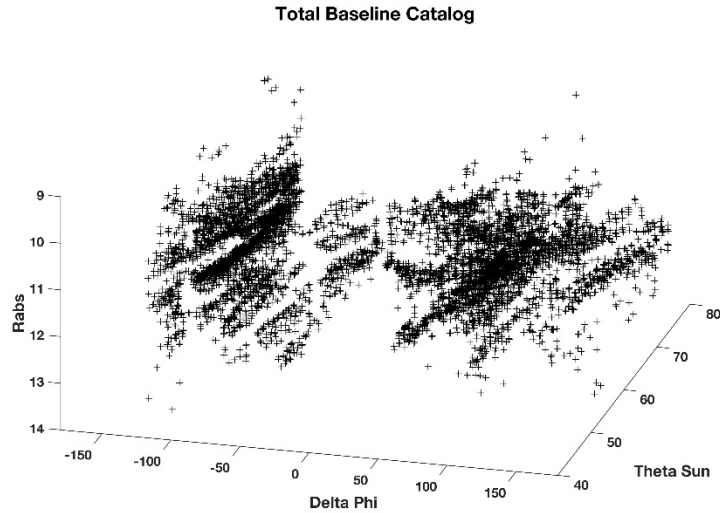
Total Baseline Catalog

Fig. 5 Three-D plot of the combined baseline catalogs

Although the DM method is based on catalogs built up from moderate-cadence observations taken during a series of whole nights, any number of new observations can be used to estimate aA$_{DM}$. Conceptually, one simply plots the new θ_s, $\Delta\Phi$, and R$_{abs}$ observations onto a plot similar to that of Fig. 5 and then finds the mean distance in magnitude between the new data point and the mean R$_{abs}$ of the nearest catalog neighbors. This magnitude difference is converted into a flux ratio, which is proportional to the aA ratio between the newly observed satellite and the mean aA of the satellites used to construct the catalog. The equation that we use is `aA = aA`$_{mean,i}$` * (0.4*10^(-`Δ`R`$_{abs}$`))`. In this equation, the subscripts "mean" and "i" indicate the mean aA value adopted for the ith of the four catalogs, and ΔR$_{abs}$ is the average difference between the new data and the catalog mean.

An example of the process is shown in Fig. 6 It illustrates most of the features of the DM method. The red plus sign markers indicate the distribution of the new data in the body-referenced coordinate system for the satellite AMC-18 on the night of Feb. 5, 2013 as seen from the Kirtland Raven. The blue circle markers indicate the mean value of the N = 25 nearest neighbors that are found in the catalog (neighbors in the θ_s and $\Delta\Phi$ coordinates). The new estimate of aA$_{DM}$ is directly calculated from the average value of the R$_{abs}$ difference between the catalog means and the new data.
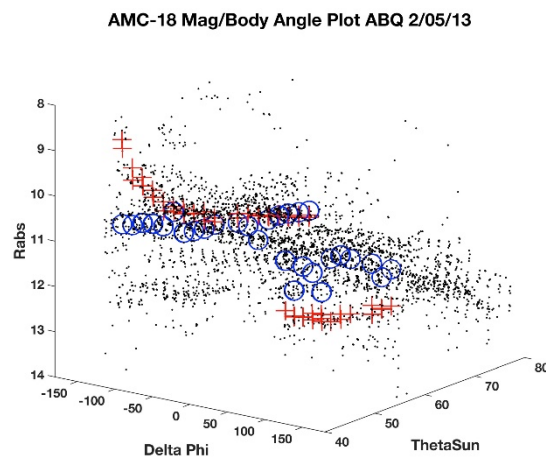
AMC-18 Mag/Body Angle Plot ABQ 2/05/13

Fig. 6 Example plot of Baseline Catalog (black), Mean of Catalog (blue circles), and New Data (red plus signs)

5. COMPARISONS BETWEEN 2FM AND DM METHODS FOR BODY aA

One problem in developing algorithms that calculate aA is there generally does not exist ground truth for this quantity. One can examine photographs and artists' conceptions in order to estimate the projected area of components when they are in orbit and then guess the albedo of the materials that appear to be important contributors of the total reflection. However, this is not very satisfactory, especially given the rather wide range of albedos for tested materials.

Given the lack of ground truth, we primarily rely on comparisons between our two methods in order to perform a low level of verification and validation. In addition to the fact that the two methods generally agree well, we add in the facts that the calculated values agree well with comparisons to web illustrations and also that the disagreements, when they do exist, agree with an analysis of the physical nature of the satellites' major components.

Table 1 presents our comparisons for the eight primary target satellites in the GOLDS1 observing campaign, which took place in the late winter and spring of 2013. Column 1 lists the common satellite name (or obvious abbreviation). Column 2 provides comments about the complexity and structure of the photometric signatures for each satellite. The single peak and triple peak objects have been discussed above. However, the two satellites, AMC-15 and AMC-18, have signatures that are of a higher complexity. During the portion of the observing campaign that took place prior to the Vernal Equinox, they each showed Double (Left) signatures, while after the equinox, they had Double (Right) signatures. This behavior is quite unusual in our experience and suggests that the com antennae on these two satellites might be mounted in planes that are tilted with respect to the Celestial Equator. Column 3 lists our best understanding of the manufacturer/bus type. The A2100 buses and derivatives are made by Lockheed Martin. The SS/L objects are made by Space Systems Loral. The BSS satellites are made by Boeing Space Systems, and the STAR 2 is made by Orbital Sciences Corp. Columns 4 and 5 list the estimated aA values resulting from the DM and 2FM methods, respectively. The quoted uncertainties are standard error of the mean. All quantities are in units of m^2.

Table 1 Comparison Between DM and 2FM Body aA Methods

Satellite	Signature Type	Bus Type	aA DM (m^2)	aA 2FM (m^2)
AMC-1	Single Peak	A2100A	1.8±0.2	1.8±0.2
AMC-15	Complex	A2100AXS	1.6±0.3	9.0±1.7
AMC-18	Complex	A2100A	9.3±1.7	19.1±1.7
DTV-8	Single Peak	SS/L 1300	2.6±0.5	1.6±0.1
DTV-9S	Trip Peak	SS/L 1300	1.9±0.4	4.1±0.5
DTV-10	Single Peak	BSS-702	4.2±0.6	2.2±0.1
SES-1	Triple Peak	Star-2.4	10.3±2.3	11.1±1.2
SPACEWAY-1	Single Peak	BSS-702	2.0±0.6	2.0±0.2

We note the four Single Peak satellites show a high level of agreement between the two body aA methods of calculation. However, the four satellites with complex signatures show much less agreement, and we see the 2FM method produces higher values of aA than the DM method does for each of these four RSOs.

6. THE SOLAR PANEL (SP) METHOD

Here we discuss and derive our method for the calculation of the Solar Panel albedo-Area (SPaA). This section is broken up into a preliminary and an algorithm section. In the preliminary section, we discuss the geometry of the problem and give details on various sub-algorithms needed for calculation for SPaA. In the algorithm section, we discuss the step-by-step process from taking a light signature and returning a value for SPaA.

6.1 THE GEOMETRY OF THE SOLAR PANEL AND ITS ALBEDO

We must consider the geometry involved with the solar panel and the incident light relative to the observer. Refer to Fig. 1 for the geometry discussed. We denote the solar panel's normal vector as $\hat{N}$. From this vector, the angle towards the Sun's incident light is labeled θ_i, and the angle towards the observer's location is denoted θ_r. The angles ϕ_i and ϕ_r are defined as the angles, in the panel's plane, going from the $x-axis$ to the projection of incident and reflected light into the panel's plane. Under the assumption that the reflected light will attain a rotational symmetry, we assume

that $\phi_i = 180°$. This is the same geometric convention used by [3]. Note that we use θ_i here in reference to the incident light to the panel's surface whereas in the body-frame we use θ_s.
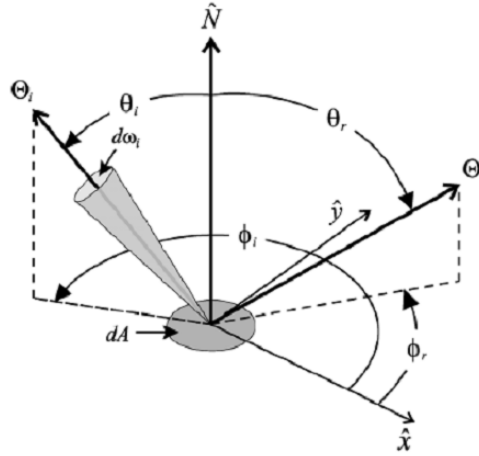

Fig. 7 The angles and vectors of the Solar Panel

The bidirectional reflectance distribution function (BRDF) is defined to be the function $f(\theta_i, \theta_r, \phi_i, \phi_r)$ which describes the scattering of radiance, reflected off of the panel's surface, in all directions above the hemisphere. This is written as:

$$f(\theta_i, \theta_r, \phi_i, \phi_r) = \frac{dL_r(\theta_r, \phi_r)}{dE(\theta_i, \phi_i)} \tag{5}$$

where L_r is the spectral radiance of the reflected light, and E is the spectral irradiance. The albedo is the total (unitless) ratio of reflected to incident light off of a given surface throughout the entire hemisphere of possible reflections. This quantity, denoted a, is defined as:

$$a = \int_0^{2\pi} \int_0^{\frac{\pi}{2}} f(\theta_i, \theta_r, \phi_i, \phi_r) \cos(\theta_r) \sin(\theta_r) \, d\theta_r \, d\phi_r. \tag{6}$$

This formula, as discussed in [3] and [2], can be derived as follows: let ω be the solid angle of reflection, and $d\omega$ be the element of the solid angle, formed by the panel reflection in the unit-hemisphere. By definition this value is a constant:

$$\omega = \int_{hemisphere} d\omega = \int_0^{2\pi} \int_0^{\frac{\pi}{2}} \sin(\theta_r) \, d\theta_r d\phi_r. \tag{7}$$

As we expect a varying albedo, we instead consider the projected solid angle, denoted Ω, and the element of projected solid angle $d\Omega$, defined as:

$$\Omega = \int_{hemisphere} d\Omega = \int_{hemisphere} \cos(\theta_r) d\omega = \int_0^{2\pi} \int_0^{\frac{\pi}{2}} \cos(\theta_r)\sin(\theta_r) \, d\theta_r d\phi_r. \tag{8}$$

Thus, our total reflectance, using a BRDF under the consideration of projected solid angles, is given by:

$$a = \int_{hemisphere} f(\theta_i, \theta_r, \phi_i, \phi_r) \, d\Omega = \int_0^{2\pi} \int_0^{\frac{\pi}{2}} f(\theta_i, \theta_r, \phi_i, \phi_r) \cos(\theta_r) \sin(\theta_r) \, d\theta_r \, d\phi_r. \tag{9}$$

6.2 CONVERSION TO OFF-REFLECTION ANGLE

Another angle used to simplify the notation is the glint angle θ^* or off-reflection angle. This is the angle from the observer to the reflection of the incident light across the panel's normal. This angle can be written as:

$$\theta^* = ArcCos[\cos(\theta_i)\cos(\theta_r) - \sin(\theta_i)\sin(\theta_r)\cos(\phi_i - \phi_r)]. \tag{10}$$

The derivation of the off-reflection angle formula is as follows: Assuming that all vectors are of unit length, let Θ_i and Θ_r be the sun and observer vectors, as in Fig. 7. We can write these vectors, along with the solar panel normal vector, $\widehat{N}$, in terms of their components with respect to the panel's plane. We assume the y direction is given by the orbital north vector, $\widehat{Orb}$, and the x direction is given by $\widehat{Orb} \times \widehat{N}$. These vectors can be now be written as:

$$\Theta_i = \begin{pmatrix} \cos(\phi_i)\sin(\theta_i) \\ \sin(\phi_i)\sin(\theta_i) \\ \cos(\theta_i) \end{pmatrix}, \quad \Theta_r = \begin{pmatrix} \cos(\phi_r)\sin(\theta_r) \\ \sin(\phi_r)\sin(\theta_r) \\ \cos(\theta_r) \end{pmatrix}, \quad and \quad \widehat{N} = \begin{pmatrix} 0 \\ 0 \\ 1 \end{pmatrix}. \tag{11}$$

We can now calculate the panel specular vector (the true reflection vector), $\widehat{P}_{spec}$, as:

$$\widehat{P}_{spec} = 2\widehat{N}(\Theta_i \cdot \widehat{N}) - \Theta_i \tag{12}$$

$$= 2\begin{pmatrix} 0 \\ 0 \\ 1 \end{pmatrix}\left(\begin{pmatrix} \cos(\phi_i)\sin(\theta_i) \\ \sin(\phi_i)\sin(\theta_i) \\ \cos(\theta_i) \end{pmatrix} \cdot \begin{pmatrix} 0 \\ 0 \\ 1 \end{pmatrix}\right) - \begin{pmatrix} \cos(\phi_i)\sin(\theta_i) \\ \sin(\phi_i)\sin(\theta_i) \\ \cos(\theta_i) \end{pmatrix}$$

$$= \begin{pmatrix} 0 \\ 0 \\ 2 \end{pmatrix}\cos(\theta_i) - \begin{pmatrix} \cos(\phi_i)\sin(\theta_i) \\ \sin(\phi_i)\sin(\theta_i) \\ \cos(\theta_i) \end{pmatrix}$$

$$= \begin{pmatrix} -\cos(\phi_i)\sin(\theta_i) \\ -\sin(\phi_i)\sin(\theta_i) \\ \cos(\theta_i) \end{pmatrix}.$$

Next, by definition, the off-reflection angle is given by the dot product of the specular and observer vectors:

$$\cos(\theta^*) = \widehat{P}_{spec} \cdot \Theta_r \tag{13}$$

$$= \begin{pmatrix} -\cos(\phi_i)\sin(\theta_i) \\ -\sin(\phi_i)\sin(\theta_i) \\ \cos(\theta_i) \end{pmatrix} \cdot \begin{pmatrix} \cos(\phi_r)\sin(\theta_r) \\ \sin(\phi_r)\sin(\theta_r) \\ \cos(\theta_r) \end{pmatrix}$$

$$= \begin{pmatrix} -\cos(\phi_i)\sin(\theta_i) \\ -\sin(\phi_i)\sin(\theta_i) \\ \cos(\theta_i) \end{pmatrix} \cdot \begin{pmatrix} \cos(\phi_r)\sin(\theta_r) \\ \sin(\phi_r)\sin(\theta_r) \\ \cos(\theta_r) \end{pmatrix}$$

$$= -\cos(\phi_i)\sin(\theta_i)\cos(\phi_r)\sin(\theta_r) - \sin(\phi_i)\sin(\theta_i)\sin(\phi_r)\sin(\theta_r) + \cos(\theta_i)\cos(\theta_r)$$

$$= -(\sin(\theta_i)\sin(\theta_r))(\cos(\phi_i)\cos(\phi_r) + \sin(\phi_i)\sin(\phi_r)) + \cos(\theta_i)\cos(\theta_r).$$

Lastly, we use the following trigonometric identity to get to the required form of θ^*:

$$\cos(A - B) = \cos(A)\cos(B) + \sin(A)\sin(B) \tag{14}$$

Applying the identity in Equation (14) to Equation (13), we get:

$$\cos(\theta^*) = -\sin(\theta_i)\sin(\theta_r)\cos(\phi_i - \phi_r) + \cos(\theta_i)\cos(\theta_r). \qquad (15)$$

After re-arranging terms and applying the inverse cosine to both sides, we arrive at the claimed formula for off-reflection angle:

$$\theta^* = ArcCos[\cos(\theta_i)\cos(\theta_r) - \sin(\theta_i)\sin(\theta_r)\cos(\phi_i - \phi_r)]. \qquad (16)$$

6.3 CALCULATING OFF-REFLECTION ANGLE FROM A SOLAR PANEL OFFSET ANGLE

Another formulation of the off-reflection angle which is needed comes from simple geometry. We assume that our signature data will be collected in terms of longitudinal phase angle, and if we also know the solar panel's correct offset angle, then we can convert our signature into brightness versus off-reflection angle (from phase angle). To see this, we define the off-reflection angle as the angle between the panel's specular reflection vector, $\vec{P}_{spec}$, and the panel to observer vector, $\overrightarrow{RO}$ (RSO to observer vector). Assuming these vectors are normalized, then, an equivalent form of (16) is:

$$\theta^* = \cos^{-1}(\hat{P}_{spec} \cdot \widehat{RO}). \qquad (17)$$

$\overrightarrow{RO}$ is the difference between the position vectors of the observer and satellite with respect to the Earth-centered frame, the panel's specular reflection vector can be calculated by:

$$\vec{P}_{spec} = \hat{N} * 2 * (\overrightarrow{RS} \cdot \hat{N}) - \overrightarrow{RS}. \qquad (18)$$

The $\overrightarrow{RS}$ vector is the difference between the position vectors of the sun and satellite, and the panel's normal vector can be found by fixing some solar panel offset angle, SPO, and calculating:

$$\hat{N} = \cos(SPO) * [(\widehat{Orb} \times \overrightarrow{RS}) \times \widehat{Orb}] + \sin(SPO) * (\widehat{Orb} \times \overrightarrow{RS}). \qquad (19)$$

Hence, if we have the solar panel's offset angle, then Equations (19), (18), and (17), in that order, give us a conversion from phase angle to off-reflection angle.

6.4 DERIVATION OF SOLAR PANEL aA

The solar panel albedo-Area is defined as the product of its albedo and its area, thus:

$$(aA)_{panel} = a\, A \qquad (20)$$

with a being the albedo and A the area of the panel in m^2. Let $g(\theta^*)$ be the "shape" of the BRDF. We assume the panel's BRDF to have a Gaussian shape, as a function of off-reflection angle, given by:

$$g(\theta^*) = e^{-2\sin^2(\theta^*)/\sigma^2} \qquad (21)$$

where σ is the width parameter of the curve and must be determined a priori (i.e., by a fitting procedure). To be used as the BRDF's shape, $g(\theta^*)$ must be normalized as to allow the BRDF to give the distribution of albedo over the hemisphere of possible observer locations. To achieve this, we define a normalizing factor G_{norm}. This constant will be the value by which the volume under $g(\theta^*)$ is normalized to 1 over the hemisphere:

$$G_{norm} = \frac{1}{\int_0^{2\pi}\int_0^{\frac{\pi}{2}} g(\theta^*)\cos(\theta_r)\sin(\theta_r)\,d\theta_r\,d\phi_r}. \qquad (22)$$

This allows for us to define our Gaussian BRDF by:

$$f(\theta^*) = a\, G_{norm}\, g(\theta^*). \tag{23}$$

Next we consider the model we are using for the panel's reflection, which consists of both specular and diffuse parts as per [1]. We estimate that the solar panel radiant intensity, measured in $\frac{W}{sr}$, would be composed of a primarily specular pattern (at least 80%), while the remaining intensity would be due to a diffuse contribution (less than 20%). This resulted in our model:

$$S_{model}(\theta^*, \theta_i, \theta_r) = C_{spec}\, Specular + C_{diff}\, Diffuse \tag{24}$$

$$\approx 0.8\, E\, A\, f(\theta^*) + 0.2\, E\, a\, A\cos(\theta_i)\cos(\theta_r)/\pi$$

where E is the in-band Solar irradiance ($E \approx 642\,\frac{W}{m^2}$ for open band). Since we are using inverse modeling, we attempt to capture the specular component of the solar panel in its entirety. This method results in the weighting constants being modified so that the panel has an entirely specular nature. That is, our model in (23) is simplified to become:

$$S_{model}(\theta^*) = 1\, Specular + 0\, Diffuse \tag{25}$$

$$= 1\, E\, A\, f(\theta^*) + 0\, E\, a\, A\cos(\theta_i)\cos(\theta_r)/\,\pi$$

$$= E\, A\, f(\theta^*).$$

Using a light curve, we attempt to fit the observed data to this model as:

$$S_{fit}(\theta^*) = P\, g(\theta^*) \tag{26}$$

for some scaling constant P. If the fit is successful, then we should have $S_{fit}(\theta^*) = S_{model}(\theta^*)$, thus resulting in:

$$S_{fit}(\theta^*) = S_{model}(\theta^*)$$

$$P\, g(\theta^*) = E\, A\, f(\theta^*)$$

$$P\, g(\theta^*) = E\, A\left(a\, G_{norm}\, g(\theta^*)\right)$$

$$P = E\, a\, A\, G_{norm}$$

$$S_{fit}(\theta^*) = P\, g(\theta^*) \tag{27}$$

which is then easily solved for the solar panel albedo-Area, units of $(aA)_{panel}$ are m^2:

$$(aA)_{panel} = a\, A \tag{28}$$

$$= \frac{P}{E\, G_{norm}}.$$

6.5 THE LINEAR FITTING METHOD (LFM)

This algorithm was developed in order to better estimate the region, in longitudinal phase angle, for the specular region of a light curve. We call it the linear fit method (LFM). For the LFM, we assume a Gaussian BRDF as in Equation (21). The fitting process is done assuming the light curve can be fit to the function $f(\theta^*) = Pg(\theta^*) = e^{a*\cos(\theta^*)+b}$. While the cosine term is equivalent to the sine squared version, we opt for the cosine form, as it provides a cleaner form to which we can fit it linearly. Using this model has a few advantages. Firstly, it is symmetric, so the sign of the off-reflection angle is irrelevant (the solar panel specular contribution to a signature is symmetric with respect to θ^*).

This means it is easy to tell where the signature is symmetric; it is symmetric where two halves of the signature, one with positive off-reflection angles and the other with negative off-reflection angles, fall on top of one another. The specular region must be within this range. Second, the equation is linear with respect to $\log(RI)$ vs $\cos(\theta^*)$, so we want to find in what region the data becomes linear when plotted as $\log(RI)$ vs $\cos(\theta^*)$, and that will be what we use as the specular region.

Using this new model, we perform an iterative search for where the two halves of the data are symmetric and linear. The specular region is centered around the off-reflection angle $\theta^* = 0$, so at each iteration we remove the same fraction, say $1/4^{th}$, of the data with the lowest off-reflection angle and process the data through LFM again. We stop once we find data that is sufficiently close to linear; checking if the data is linear incorporates a check for if the data is symmetric because if two halves do not fall on top of each other, then the data cannot be linear. In order to check if the data is linear, we fit the data with the linear fit produced by the observation points with the largest and smallest off-reflection angle. If any of the remaining points are further from the fitted line than some predetermined distance, then the data is not sufficiently linear, and the next iteration of the algorithm is executed. Once the data that is linear satisfies our maximum distance bound, we use the fitted line produced by the observations with the largest and smallest off-reflection angles as the specular fit for the data. A flow chart of the algorithm can be seen in Fig. 8.
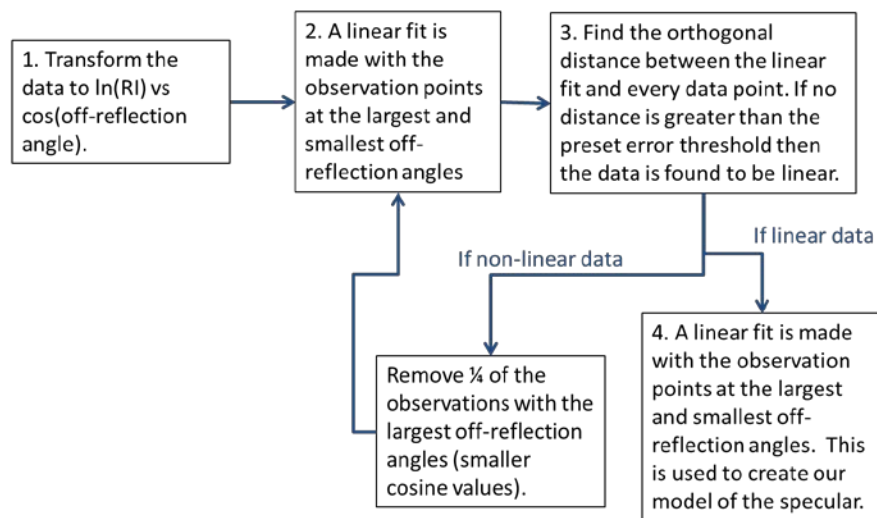

Fig. 8 Flowchart of the linear fitting algorithm

Fig. 9 shows an example run of the algorithm. Each red line represents one iteration of LFM. For a given iteration, all of the data with smaller off-reflection angles (larger cosine values) than the line is used for the fit. This process occurs from left to right, so the first iteration is represented by the left most line, the second by the line directly to the right of that, and so on. The data to the right of the rightmost line represents the data that was found to be linear "enough"; the linear fit between the observation points with the largest and smallest off-reflection angles in that range of data is used as the fit for the model. The process stops once this maximum distance is reached.
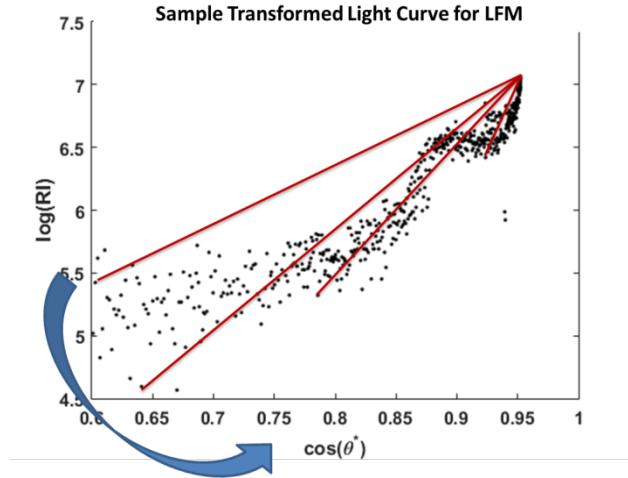
Fig. 9 Example run of linear fit algorithm on a light curve

The final line from LFM, whose equation can be given as $y = m\cos(\theta^*) + b$, allows for the Gaussian parameters in (27) to be estimated by $P = e^{m+b}$ and $\sigma^2 = \frac{1}{m}$.

6.6 THE SOLAR PANEL METHOD ALGORITHM

The process of generating the solar panel albedo-Area takes three stages to complete. First, a solar panel offset angle must be correctly identified. This is the angle between the solar panel's normal vector and the sun. Second, using the correct offset angle allows for the light curve to be converted from longitudinal phase angle to off-reflection angle. Finally, in the off-reflection angle space, the linear fitting method allows for a Gaussian fit to be made to the data whose parameters allow for SPaA to be calculated.

The overall process occurs in the following manner with regard to a single light curve which we assume to be data collected in radiant intensity, RI, in units of $\frac{W}{sr}$, vs longitudinal phase angle:

1. Obtain correct solar panel offset (SPO) angle.
    a. Create a set SPO guesses in the range of $[-30°, 30°]$.
    b. For each SPO guess, calculate the light curve's off-reflection angles, θ^*, by (17).
    c. Use the LFM to approximate a specular region in terms of θ^*, for each SPO guess. Denote this region by $[-\theta^*_{spec}, \theta^*_{spec}]$.
    d. Within the specular region, $[-\theta^*_{spec}, \theta^*_{spec}]$, we fit a quadratic function, $A\theta^{*2} + B\theta^* + C$, to the graph of $\log(RI)$ vs θ^*. Recall that we assume the brightness, RI, to have a Gaussian shape inside the specular region.
    e. Record each value of the quadratic B for each SPO guess.
2. Obtain the correct set of off-reflection angles.
    a. Use a root finding algorithm to find the root of all values of quadratic B versus the SPO guesses. The SPO which provides a value of $B = 0$ will be the panel's true offset angle, SPO_o.
    b. Use SPO_o to obtain the signature's true off reflection angles by (17).
3. Calculate SPaA.
    a. For the off-reflection angles obtained with the correct offset SPO_o, use the LFM to obtain Gaussian parameters (P and σ) for Equation (27).
    b. Numerically integrate G_{norm} from Equation (22).
    c. Plug the values of $P, \sigma,$ and G_{norm}, in to (28) to obtain the solar panel albedo-Area.

6.7 SOLAR PANEL aA RESULT SUMMARY FOR USNO DATASET

Here we present a summary of our results on the solar panel albedo-Areas found by the method presented. The photometric observation data was collected by sensors over the course of two years starting in 2013. The mean aA values shown in Table 2 are averages over all light curves returning a value as some nights do not contain enough data to produce a meaningful value.

Table 2 Solar panel aA results for several GEO satellites

Satellite Name	Bus Type	Mean Solar Panel albedo-Area (m^2)
AMC-1 (GE-1)	LM A2100A	6.6
AMC-7 (GE-7)	LM A2100A	4.4
Galaxy-12	Star-2	8.5
Horizons-1 (Galaxy-13)	BSS 601-HP	13.0
AMC-10 (GE-10)	LM A2100A	4.7
AMC-11 (GE-11)	LM A2100A	6.0
Galaxy-14	Star-2	5.4
Galaxy-15	Star-2	5.4
AMC-21	Star-2	11.4
CIEL-2	Spacebus 4000C4	13.3
GOES-15	BSS 601-HP	15.8

7. DISCUSSION AND CONCLUSION

We have presented results on one new algorithm (DM) and one algorithm under continuing development (2FM) for extracting the albedo-Area of the satellite body alone. For those satellites with simple signatures (i.e., one central brightness peak located near PA = 0º), the agreement between the two methods is quite good. However, for those objects with more complex signatures (i.e., those with broad shoulders or secondary peaks that are located in the general range of 20º < abs(PA) < 40º), we find that the two methods disagree and that the 2FM method estimates the body aA as larger than the DM method does.

There is an explanation for the disagreements. First, the DM method excludes brightness data that lies in the range abs(PA) < 40º, whereas the 2FM method often includes brightness data that lies in the range 20º < abs(PA) < 40º. The inclusion of data that is closer to the central PA regime does not affect the single peak signature objects because the bright near-specular solar panel reflections do not encroach on the PA range of either method in such signatures. However, for those satellites that show side peaks or shoulders, the "excess" brightness does often fall in the PA range of the 2FM method (cf. Fig. 3 and Fig. 4). These differences do not strike us as flaws in either method. Indeed, we believe that it might be possible to exploit the differences in a manner that allows for a richer set of features that can be gleaned and thereby provide for better SSA analyses. The differences between the DM and 2FM methods, to the best of our current interpretation of the data, lie in whether or not a substantial portion of the reflected light of the com antennae are included in the aA calculation. Hence the DM estimates of aA appear to be more directly related to characterize the size of the main body/payload of the satellite, while the 2FM estimates of aA appear to be more directly related to the body/payload *plus* the com antennae. We are currently evaluating whether or not these differences can be fully exploited.

Another new algorithm has been developed and tested for estimating the albedo-Area of the solar panels based on the specular contribution of the overall reflected intensity from the satellite. The diffuse contribution from solar panels, by their design and function, is negligibly low and so is ignored in this approach. The sizes of the solar panels vary with satellite design and type of solar panel material. The areas can range from 12 to 70 m^2 for the satellites we have studied. Since albedo is less than one, reflectance aAs are only proxies for the true physical size. Further research might indicate if the aAs can be studied over time to determine effects of space weather on the reflectivity of the materials.

The accuracy of these approaches for estimating the component aAs is dependent on sampling the various parts of the satellite well. Research continues to understand the effects of sparse data on the resulting aAs. Another challenge in validating these approaches is the availability of truth data. Our research group has been using satellite model dimensions as a proxy for truth data.

One future area of work is to investigate the use of splines for improving the fit of the specular regions of the signatures. If improvements to the fits are shown, this would improve both the solar panel offset calculation and the solar panel aA. Another area of work will be to investigate how to fuse the DM and 2FM methods for improved body aA estimation with sparse data and possibly to quantify the contribution of the antennae.

8. REFERENCES

1. Montenegro, E. S., Hocmuth, D. H., & Hartley, T. R. (2006). *Optical Signatures Code.* Special Report, Teledyne Solutions, Inc., Huntsville, Alabama.
2. Nicodemus, F. E., Richmond, J. C., Hsia, J. J., Ginsberg, I. W., & Limperis, T. (1977). *Geometrical Considerations and Nomenclature for Reflectance.* National Bureau of Standards, Department of Commerce. Washington, D.C.: Department of Commerce, National Bureau of Standards.
3. Shell, J. R. (2004). *Bidirectional Reflectance: An Overview with Remote Sensing Applications & Measurement Recommendations.* Rochester Institute of Technology, Center for Imaging Science, Rochester, New York. Retrieved from http://web.gps.caltech.edu/~vijay/Papers/BRDF/shell-04.pdf